

A PHYSICAL MODEL OF Ly $\alpha$  EMITTERSVITHAL TILVI<sup>1</sup>, SANGEETA MALHOTRA<sup>1</sup>, JAMES E. RHOADS<sup>1</sup>, EVAN SCANNAPIECO<sup>1</sup>, ROBERT J. THACKER<sup>2</sup>, ILIAN T. ILIEV<sup>3,4</sup>, AND GARRELT MELLEMA<sup>5</sup>

## ABSTRACT

We present a simple physical model for populating dark matter halos with Ly $\alpha$  emitters (LAEs) and predict the properties of LAEs at  $z \approx 3 - 7$ . The central tenet of this model is that the Ly $\alpha$  luminosity is proportional to the star formation rate (SFR) which is directly related to the halo mass accretion rate. The only free parameter in our model is then the star formation efficiency (SFE). An efficiency of 2.5% provides the best fit to the Ly $\alpha$  luminosity function (LF) at redshift  $z = 3.1$ , and we use this SFE to construct Ly $\alpha$  LFs at other redshifts. Our model reproduces the Ly $\alpha$  LFs, stellar ages,  $\text{SFR} \approx 1 - 10 M_{\odot} \text{ yr}^{-1}$ , stellar masses  $\sim 10^7$  to  $10^8 M_{\odot}$ , and the clustering properties of LAEs at  $z \approx 3 - 7$ . We find the spatial correlation lengths  $r_o \approx 3 - 6 h^{-1} \text{ Mpc}$ , in agreement with the observations. Finally, we estimate the field-to-field variation  $\approx 30\%$  for current volume and flux limited surveys, again consistent with observations. Our results suggest that the star formation, and hence Ly $\alpha$  emission in LAEs can be powered by accretion of new material. Relating the accreted mass, rather than the total mass, to the Ly $\alpha$  luminosity of LAEs naturally gives rise to their duty cycle.

*Subject headings:* accretion, accretion disks-dark matter-galaxies: high-redshift — galaxies: Lyman alpha emitters — galaxy: luminosity function, mass function galaxy: clustering — galaxy: correlation length

## 1. INTRODUCTION

Ly $\alpha$  emitting galaxies (LAEs) are selected on the basis of strong Ly $\alpha$  emission line, irrespective of other galaxy properties (e.g. Cowie & Hu 1998; Rhoads et al. 2000; Rhoads & Malhotra 2001; Rhoads et al. 2004; Fynbo et al. 2001; Ajiki et al. 2003; Matsuda et al. 2005; Taniguchi et al. 2005; Wang et al. 2005; Gawiser et al. 2006; Shimasaku et al. 2006; Tapken et al. 2006; Murayama et al. 2007; Nilsson et al. 2007; Ouchi et al. 2008). However, high-redshift galaxies selected on the basis of this one property are reasonably uniform in some of their other properties<sup>6</sup>. For example, the inferred stellar mass of LAEs at  $z < 5$  is typically small,  $\sim 10^6$  to  $10^9 M_{\odot}$  (Gawiser et al. 2006; Pirzkal et al. 2007; Finkelstein et al. 2007; Pentericci et al. 2009) and they often have large Ly $\alpha$  equivalent width (EW) indicating a young stellar population (Malhotra & Rhoads 2002), which is also supported by the blue color of these galaxies (Venemans et al. 2005; Finkelstein et al. 2007, 2008; Gawiser et al. 2006; Pirzkal et al. 2007) especially at high redshifts. Active galactic nuclei (AGNs) are ruled out as sources of strong Ly $\alpha$  emission in LAEs due to non-detection of X-ray emission (Malhotra et al. 2003; Wang et al. 2004; Gawiser et al. 2007) and the

lack of high ionization lines in the optical spectra (Dawson et al. 2004, 2007; Wang et al. 2009). LAEs have moderate SFRs  $\approx 5\text{--}8 M_{\odot} \text{ yr}^{-1}$  (e.g. Pirzkal et al. 2007; Taniguchi et al. 2005) and spatial correlation lengths of  $\approx 3 - 5 h^{-1} \text{ Mpc}$ , albeit with a substantial uncertainty (Ouchi et al. 2003; Kovač et al. 2007; Gawiser et al. 2007).

Despite the increasing number of LAE observations, theoretical understanding of LAEs is still in early stages, primarily due to a poor understanding of physical properties including star formation, stellar initial mass function, Ly $\alpha$  escape fraction, and the duty cycle of the Ly $\alpha$  phase. There have been several theoretical studies of LAEs based on cosmological simulations (e.g. Barton et al. 2004; Davé et al. 2006; Tasitsiomi 2006; Shimizu et al. 2007; Nagamine et al. 2008), semi-analytical models (e.g. Le Delliou et al. 2006; Kobayashi et al. 2007, 2009; Dayal et al. 2008; Samui et al. 2009) and analytical models (e.g. Haiman & Spaans 1999; Dijkstra et al. 2007; Mao et al. 2007; Stark et al. 2007; Fernandez & Komatsu 2008) that relate the total halo mass to the Ly $\alpha$  luminosity of LAEs. Such a linear relationship between the halo mass and Ly $\alpha$  luminosity often leads to an overprediction of the number density of LAEs. To reconcile the mass distribution of halos to the luminosity function (LF), one needs to either assume a small escape fraction of Ly $\alpha$  photons (which fails to account for the large Ly $\alpha$  EWs observed) or introduce a duty cycle (e.g. Stark et al. 2007; Nagamine et al. 2008) which adds another parameter to the models. In addition, the complexity and large number of variable parameters in many models motivate the development of a simple approach, which is particularly useful in understanding the nature of LAEs observed at high redshifts.

In this paper, we present a physical model to popu-

<sup>1</sup> School of Earth and Space Exploration, Arizona State University, Tempe, AZ 85287 ; tilvi@asu.edu

<sup>2</sup> Saint Mary's University, Halifax, NS, Canada, B3H 3C3.

<sup>3</sup> Universitaet Zuerich, Institut fuer Theoretische Physik, CH-8057 Zuerich, Switzerland.

<sup>4</sup> Astronomy Centre, Department of Physics & Astronomy, Penvensey II Building, University of Sussex, Falmer, Brighton BN1 9QH, United Kingdom.

<sup>5</sup> Dept. of Astronomy and Oskar Klein Centre, AlbaNova, Stockholm University, SE-10691 Stockholm, Sweden

<sup>6</sup> In this paper we restrict our studies to only compact LAEs (at  $z = 3 - 6.6$ ) detected using narrow-band excess. Other Ly $\alpha$  emitting objects (e.g. Ly $\alpha$  blobs and AGNs) are typically much more energetic and are probably fueled by AGN activity.

late dark matter (DM) halos with LAEs in a cosmological simulation, and predict the abundances and physical properties at  $z \approx 3-7$ . This model differs fundamentally from many of the earlier studies in that we relate mass accreted, as opposed to the total halo mass, to the Ly $\alpha$  luminosity. Mass accretion onto halos via smooth infall and accretion due to mergers of a specific mass ratios has been shown to have distinctly different clustering behavior (Scannapieco & Thacker 2003). However, in our current work we do not distinguish between smooth accretion and the accretion due to mergers. In other words, in our model the LAEs are undergoing an episode of star formation driven by accretion of fresh material onto the halos, independent of whether the accretion is due to mergers or via smooth infall. While there is no direct observational evidence showing a relation between the baryons accreted and the Ly $\alpha$  luminosity, recent studies (e.g. Dekel et al. 2009; Kereš et al. 2009) have shown that such cold accretion of new material can drive star formation in galaxies.

Using the Millennium simulation, Genel et al. (2008) found that the high SFRs observed in  $z \approx 2$  galaxies can be explained by continuous mass accretion. Similar studies (e.g. Haiman et al. 2000; Fardal et al. 2001) have shown that the baryons inside high-redshift halos can release significant amount of gravitational binding energy in the form of Ly $\alpha$  luminosity as the baryons condense within DM potential wells. The Ly $\alpha$  emission resulting from this mechanism would, however, lead to low surface brightness extended Ly $\alpha$  emitters or Ly $\alpha$  blobs which are more diffuse than LAEs.

In this model, we assume that LAEs do not contain large amounts of dust, and hence most of the hydrogen ionizing photons will be absorbed, while most of the Ly $\alpha$  photons will escape (Gawiser et al. 2006; Kobayashi et al. 2007). These assumptions are needed to produce large EWs of Ly $\alpha$  line (Malhotra & Rhoads 2002). It has also been shown that the velocity gradients in the gas can facilitate the Ly $\alpha$  photon escape and making them less susceptible to dust absorption (Dijkstra et al. 2006). In addition, Ly $\alpha$  photons can preferentially escape from LAEs if the dust is primarily in cold, neutral clouds (Haiman & Spaans 1999; Hansen & Oh 2006; Finkelstein et al. 2008). Our assumption of large escape fraction of Ly $\alpha$  photons naturally yields large Ly $\alpha$  EWs even without appealing to metal-free Population III stars, whose contributions are constrained by non-detection of the He II (1640) line (Dawson et al. 2004, 2007; Nagao et al. 2008; Wang et al. 2009). In such conditions, the Ly $\alpha$  line becomes a direct measure of the SFR, which is proportional to the accretion of fresh gas onto the galaxy. The constant of proportionality (the star formation efficiency, SFE) between accretion rates and Ly $\alpha$  luminosity is the only free parameter in our model.

This paper is organized as follows. In Section 2, we give a detailed description of our physical model. We describe the DM simulation parameters, and how we generate DM halo catalogs in Section 3. In Section 4, we first construct Ly $\alpha$  LF using model LAEs at  $z \approx 3$  and compare it to the observations to find the best-fit model parameter, and then use this best-fit parameter to construct Ly $\alpha$  LFs at  $z > 3$ . In Section 5, we derive the physical properties of LAEs using our best-fit model, es-

timate the dust mass in our model LAEs to compare with the dust estimates from observations, construct UV LF of our model LAEs and compare it with the observations, and then investigate the evolution of Ly $\alpha$  LF. We study the large-scale structure of model LAEs, and study the redshift evolution of correlation lengths of LAEs in Section 6. We summarize and present conclusions in Section 7.

## 2. PHYSICAL MODEL FOR Ly $\alpha$ EMITTERS

Our model is motivated by the idea that Ly $\alpha$  emission in LAEs is associated with star formation (Partridge & Peebles 1967) from rapid accretion of new material on to the DM halos. This new material provides fresh fuel to the system driving the star formation (Kereš et al. 2009).

We populate each DM halo with an LAE, and assign to it Ly $\alpha$  luminosity ( $L_{Ly\alpha}$ ) proportional to the SFR using the following equation:

$$L_{Ly\alpha} = 1 \times 10^{42} \times \frac{SFR}{M_{\odot} \text{yr}^{-1}} \text{ erg s}^{-1}. \quad (1)$$

Here  $L_{Ly\alpha}$  is the intrinsic luminosity of an LAE. The observed Ly $\alpha$  flux will also depend on the escape fraction of the Ly $\alpha$  photons ( $f_{esc}^{Ly\alpha}$ ). Moreover, equation (1) implicitly assumes an escape fraction near zero for the ionizing continuum photons, whose absorption is required to produce the Ly $\alpha$  emission line.

While the escape fraction of ionizing Lyman continuum photons ( $\lambda < 912 \text{ \AA}$ ) is not very precisely known, several studies have shown that an escape fraction of only a few percent is sufficient to meet the observational constraints on the reionization epoch (e.g. Wood & Loeb 2000; Hansen & Oh 2006; Razoumov & Sommer-Larsen 2006; Gnedin et al. 2008). In addition, observations are also generally consistent with small escape fractions of Lyman continuum photons both locally (Leitherer et al. 1995) and at high redshifts (e.g. Hansen & Oh 2006; Shapley et al. 2006).

The escape fraction of Ly $\alpha$  photons ( $f_{esc}^{Ly\alpha}$ ) is likely to be large with  $f_{esc}^{Ly\alpha} \approx 1$  causing the large observed Ly $\alpha$  EWs (Malhotra & Rhoads 2002; Finkelstein et al. 2007; Wang et al. 2009). However, the semi-analytic model of Le Delliou et al. (2006) predicts a much smaller value of  $f_{esc}^{Ly\alpha} = 2\%$  which is compensated by top-heavy initial mass function in their model. For simplicity, in our model we approximate  $f_{esc}^{Ly\alpha}$  and Lyman continuum photons as unity and zero, respectively. Thus, all the Ly $\alpha$  photons produced in LAEs escape to be observed while none of the ionizing photons escape from the galaxy. Small deviations from these assumptions will not affect our results significantly.

As stated earlier, in our model we assume that the accretion of new material on to DM halos causes star formation in LAEs. We estimate the SFR, *i.e.* the mass in accreted gas  $\Delta M_{gas}$  converted to stars in unit time, in LAEs by converting baryonic mass accreted ( $\Delta M_b$ ) by DM halos, adopting a constant ratio of baryons to the DM, over a short timescale,  $t_{Ly\alpha}$ . This timescale ( $\approx 30 \text{ Myr}$ ) is broadly similar to the stellar population ages of most Ly $\alpha$  galaxies (e.g. Pirzkal et al. 2007; Finkelstein et al. 2007, 2008), the lifetimes of OB associations, and the dynamical time expected for Ly $\alpha$  galaxies

based on their measured sizes (Pirzkal et al. 2007). In addition, the dust produced in supernovae (SNe), which occurs approximately on timescales of  $\sim 30$  Myr, may reduce the fraction of Ly $\alpha$  photons escaping from LAEs, thus giving rise to the duty cycle of LAEs (Kovač et al. 2007), which is also reproduced in our model. A similar timescale ( $\approx 70$  Myr) was used by Shimizu et al. (2007) to match the morphology of large-scale structure of LAEs by varying the amplitude of density fluctuations in galaxy formation models.

Thus,

$$SFR = f_{\star} \times \left( \frac{\Delta M_{gas}}{t_{Ly\alpha}} \right) = f_{\star} \times \left( \frac{\Delta M_b}{t_{Ly\alpha}} \right) = f_{\star} \times \dot{M}_b, \quad (2)$$

where  $f_{\star}$  is the SFE. In the above equation, we have assumed that  $\Delta M_{gas}$  is same as the baryonic mass accreted ( $\Delta M_b$ ) by the DM halos, and since our simulation contained only DM particles, we use the universal ratio of baryonic and DM densities *i.e.*,  $\Delta M_b = (\Omega_b/\Omega_{DM}) \times \Delta M_{DM}$ , where  $\Omega_b$  and  $\Omega_{DM}$  are the baryonic and DM density parameters and  $\Delta M_{DM}$  is the dark matter mass accreted by the DM halos.

Finally, the total mass in young stars in a LAE, is estimated using

$$M_{\star} \approx SFR \times t_{Ly\alpha} = f_{\star} \times \dot{M}_b \times t_{Ly\alpha} = f_{\star} \times \frac{\Omega_b}{\Omega_{DM}} \times \Delta M_{DM}. \quad (3)$$

This corresponds to the mass of stars younger than 30 Myr which contribute to the Ly $\alpha$  and UV continuum emission, which is more easily measured than the total stellar mass. The only unknown variable in all of the above equations is  $f_{\star}$ , the only free parameter in our model. Here we note that  $f_{\star}$  and  $\Omega_b/\Omega_{DM}$  ratio in the above equations are degenerate and these values may vary somewhat for individual galaxies.

### 3. SIMULATION & HALO CATALOGS

We constructed the DM halo catalog using an N-body DM cosmological simulation code GADGET2 (Springel 2005). We generated the initial conditions for the simulation using second-order Lagrangian Perturbation Theory (Crocce et al. 2006; Thacker & Couchman 2006). In this simulation we use  $1024^3$  DM particles in a co-moving volume of  $(102 \text{ Mpc})^3$ , a volume greater than a typical LAE survey. Each DM particle has a mass  $\approx 2.7 \times 10^7 M_{\odot} h^{-1}$ . Using a Friends-of-Friends (FOF) halo finder (Davis et al. 1985), we identify DM halos that contain 100 or more DM particles. This corresponds to a minimum halo mass  $\approx 2.7 \times 10^9 M_{\odot} h^{-1}$ . We then generate catalogs, for redshifts from  $z = 10$  to  $z = 3$ , which contain positions of halos, their DM mass, and unique IDs of each individual particle that belongs to a given halo. These unique particle IDs are later used to track halos between two epochs. Throughout this work we assumed a flat  $\Lambda$ CDM cosmology with parameters  $\Omega_m=0.233$ ,  $\Omega_{\Lambda}=0.721$ ,  $\Omega_b=0.0462$ ,  $h=0.71$ ,  $\sigma_8=0.817$  where  $\Omega_m$ ,  $\Omega_{\Lambda}$ ,  $\Omega_b$ ,  $h$ , and  $\sigma_8$  correspond, respectively, to the matter density, dark energy density, and baryonic density in units of the critical density, the Hubble parameter in units of  $100 \text{ km s}^{-1} \text{ Mpc}^{-1}$ , and the RMS density fluctuations on the  $8 \text{ Mpc } h^{-1}$  scale, in agreement with WMAP (Spergel et al. 2007) five year

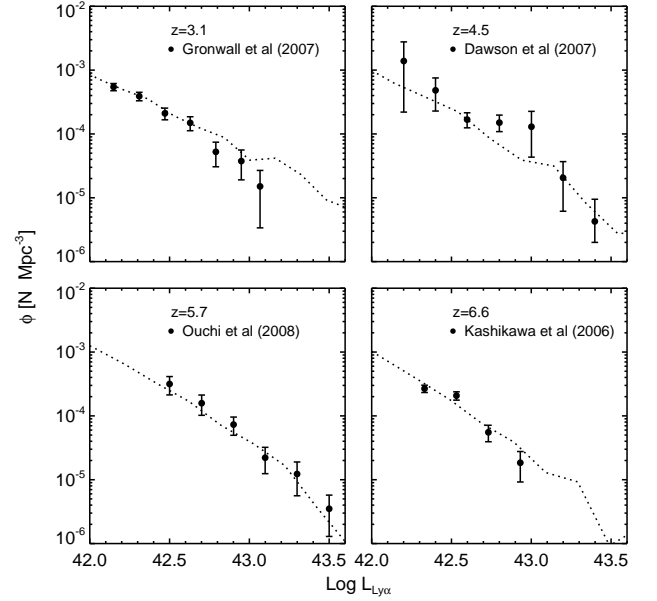


FIG. 1.— Evolution of Ly $\alpha$  LFs at redshifts  $z \approx 3 - 7$ . The dotted lines show results from our model and the symbols with error bars are the observational data. (a) The best-fit model Ly $\alpha$  LF at  $z = 3.1$  yields a SFE of 2.5%. We use this SFE to construct model Ly $\alpha$  LFs at  $z=4.5$ , 5.7, and 6.6 (b)-(d). The references for the data:  $z = 3.1$  (Gronwall et al. 2007),  $z = 4.5$  (Dawson et al. 2007),  $z = 5.7$  (Ouchi et al. 2008), and  $z = 6.6$  (Kashikawa et al. 2006).

results (Hinshaw et al. 2009).

### 4. LYMAN ALPHA LUMINOSITY FUNCTION

We now construct the Ly $\alpha$  LF, the number of LAEs per unit volume in a given luminosity bin. First, we calculate the total DM mass accreted ( $\Delta M_{DM}$ ) by each DM halo at  $z = 3.1$  during an interval  $\approx 30$  Myr (equals  $t_{Ly\alpha}$  in equation (2)). To calculate  $\Delta M_{DM}$  we track each halo, using the unique ID associated with particles in a given halo, between two epochs separated in time  $t_{Ly\alpha}$ . In general, we expect every halo to accrete more mass with time. However, due to group finding noise, we find that some halos lose mass (negative mass accretion) between outputs. In other words, the mass accretion by some halos is not real but results from the simulation noise. The main reason for this noise is the way halos are identified in any DM simulation.

In our DM simulation, we use a FOF halo finder which links all the particles within a linking length from each other into a halo, independent of whether a given particle is gravitationally bound to a halo. Thus, associating a particle with a halo based on the linking length gives rise to some uncertainty in halo mass (in this case  $\Delta M_{DM}$ ). To determine how many halos have real accretion, rather than spurious apparent accretion due to uncertainty in particle association with a halo by the halo finder, we first construct a histogram of  $\Delta M_{DM}$  including the halos with negative  $\Delta M_{DM}$ . We then subtract the halo counts in negative  $\Delta M_{DM}$  bins from the corresponding counts in the positive  $\Delta M_{DM}$  bins. This procedure compensates for halos that show accretion just due to random nature of a FOF halo finder. The remaining halos with positive accretion rates are then considered for constructing Ly $\alpha$

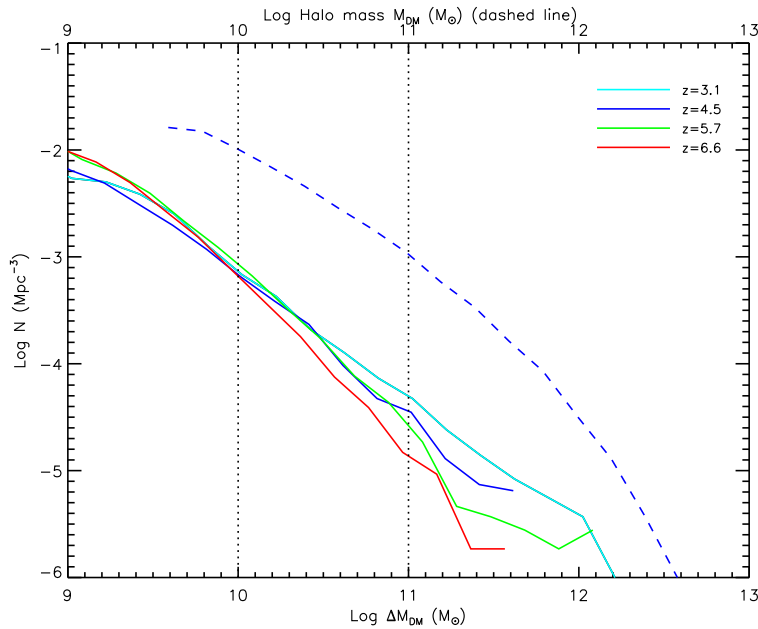


FIG. 2.— Accreted mass function and halo mass functions. Solid lines show accreted mass functions at  $z = 3.1$  (violet),  $z = 4.5$  (blue),  $z = 5.7$  (green) and  $z = 6.6$  (red). The dashed blue line shows the dark matter halo mass functions at  $z = 4.5$  to compare with the corresponding accreted mass function. The vertical dotted lines enclose the region of observed Ly $\alpha$  luminosities in LAEs.

LFs.

Next, we convert the accreted mass bins to the Ly $\alpha$  luminosity bins using equation (1) to yield Ly $\alpha$  LF. We then compare this LF with the observations at  $z = 3.1$  (Gronwall et al. 2007), and get the best-fit model by varying the SFE ( $f_\star$ ) to yield the least reduced  $\chi_r^2$  ( $\chi^2$  per degree of freedom) given by

$$\chi_r^2 = \frac{1}{N-1} \sum \frac{(N_{model} - N_{obs})^2}{\sigma_{model}^2 + \sigma_{obs}^2}, \quad (4)$$

where  $N$ ,  $N_{model}$  &  $N_{obs}$  are the number of observed data points, LAE counts from model, and the observed LAE counts in each bin, respectively, and the Poisson errors are given by  $\sigma_{model} = \sqrt{N_{model}}$  and  $\sigma_{obs} = \sqrt{N_{obs}}$ . Figure 1 (top left) shows the best-fit model Ly $\alpha$  LF (dotted line) at  $z = 3.1$ . The symbols are the observations from Gronwall et al. (2007) shown with  $1\sigma$  error bars.

Lastly, we use the best-fit model parameter  $f_\star$  i.e., the SFE at  $z = 3.1$  to construct the model Ly $\alpha$  LFs at  $z > 3$ , and then compare these LFs with the observations at  $z = 4.5$ , 5.7, and 6.6. Figure 1 shows the Ly $\alpha$  LFs from our model (dotted lines) and observations (filled circles) at redshifts  $z = 3.1$  (Gronwall et al. 2007),  $z = 4.5$  (Dawson et al. 2007),  $z = 5.7$  (Ouchi et al. 2008), and  $z = 6.6$  (Kashikawa et al. 2006). We have rebinned the observational data for  $z = 3.1$  and  $z = 6.6$  data so as to make the bin size uniform at all redshifts. Wiggles seen, especially in the  $z = 4.5$  model Ly $\alpha$  LF (Figure 1, top right) are probably due to statistical noise. The best-fit model for  $z = 3.1$  Ly $\alpha$  LF yields a SFE of 2.5%. Corresponding to this SFE, the  $\chi_r^2$  values between our model and the observed Ly $\alpha$  LFs are 0.5, 0.8, 1.2 & 1.5 for Ly $\alpha$  LFs at  $z = 3.1$ , 4.5, 5.7, and 6.6, respectively.

## 5. RESULTS

Our model Ly $\alpha$  LFs with single SFE, agree remarkably well with the observations (Dawson et al. 2007;

Ouchi et al. 2008). They reproduce, without any additional parameters, the duty cycle of  $\sim 10\%$  obtained from clustering studies (Kovač et al. 2007). To predict the Ly $\alpha$  LFs of LAEs, Nagamine et al. (2008) investigated two models, the duty cycle and escape fraction scenario, and found that the duty cycle model reproduces observations better than the escape fraction model. In our model, the duty cycle is naturally produced since only halos with high accretion rates will be observed as LAEs. Figure 2 shows the halo mass function at  $z = 4.5$  (blue dashed line) and the accreted mass function (blue solid line). Thus, the use of accreted mass rather than the total halo mass eliminates the need to introduce an additional duty cycle parameter in our model.

LAE observations at high redshifts suggest that many of the properties of LAEs such as the LFs do not evolve significantly over a wide redshift range (Dawson et al. 2007; Ouchi et al. 2008). These observations are in agreement with our model predictions, i.e., our model predicts nearly a constant SFE over a wide redshift range and that other physical properties including Ly $\alpha$  luminosity, and SFRs do not evolve significantly from  $z \approx 3$  to 7 since, in our model, these properties depend on SFE. Jimenez et al. (2005) also found a similar constant SFE over a wide range ( $\approx 2$  orders of magnitude) of stellar masses, and over a relatively large redshift range, using a large SDSS spectroscopic sample of galaxies at  $z < 0.3$ , combined with stellar population models. Figure 3 shows the DM accretion rate as a function of halo mass. The solid line is the least-square fit to the median mass in a  $\Delta M/dt$  bin. A nearly constant (0.8-0.9) slope of this line at all redshifts implies that the SFR does not evolve in this redshift range, while deviation of the slopes from unity suggests that the mass accretion rate is a nonlinear function of halo mass. Using least-square fits to the median mass in each  $\Delta M/dt$  bin (Figure 3), we obtain

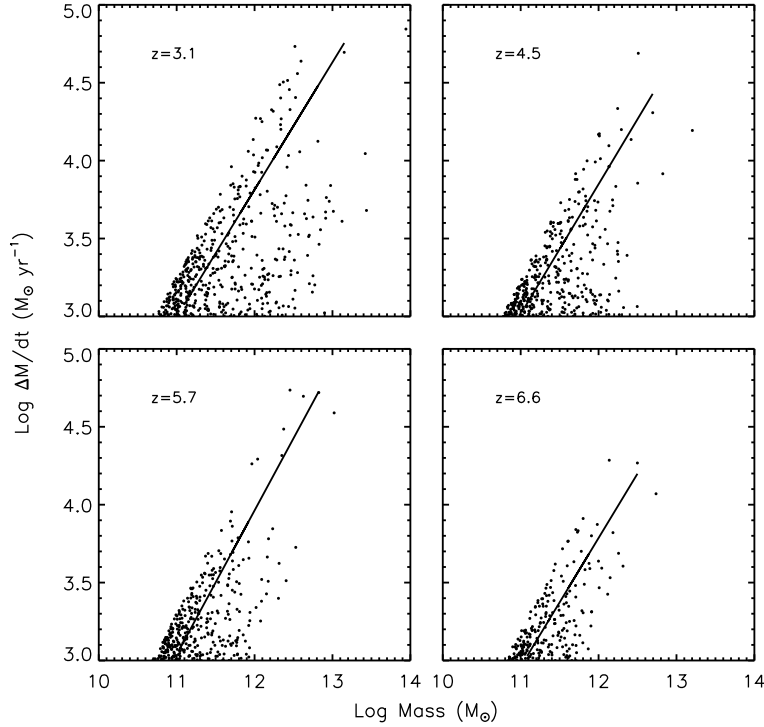


FIG. 3.— The DM accretion rate of halos as a function of halo mass at  $z \approx 3 - 7$ . The solid line is the least-square fit to the median mass in each  $\Delta M/dt$  bin. The slope of the lines is nearly constant  $\approx 0.8 - 0.9$  over all redshifts.

an average DM mass accretion rate  $\Delta M/dt$ ,

$$\frac{\Delta M}{dt} \approx 4.3 \times 10^{-7} M_{\text{DM}}^{0.85} M_{\odot} \text{yr}^{-1}, \quad (5)$$

where  $M_{\text{DM}}$  is the DM halo mass. For example, for a halo mass of  $10^{11} M_{\odot}$ , the baryonic mass accretion rate, obtained by converting DM mass accretion rate using universal ratio of baryons to DM, is approximately  $170 M_{\odot} \text{yr}^{-1}$ .

### 5.1. Physical properties of LAEs

We use the best-fit model parameter (SFE) at  $z = 3.1$  to derive other physical properties of LAEs and compare our results with the observations. Our best-fit model yields an SFE of 2.5%, consistent with the global SFE. Fukugita et al. (1998) predicted a SFE  $< 5\%$ , while Baldry et al. (2008) found this value in the range 4%–8% for blue light in galaxies. While our model predicts a roughly constant SFE over a wide redshift range, in reality this value will vary somewhat depending on the ratio of baryons to DM.

The SFE of 2.5% yields SFRs  $\approx 1 - 10 M_{\odot} \text{yr}^{-1}$  corresponding to the observed Ly $\alpha$  luminosity range  $L_{\text{Ly}\alpha} \approx 1 \times 10^{42} - 1 \times 10^{43} \text{ erg s}^{-1}$ . This SFR is comparable to the inferred SFR  $\approx 8 M_{\odot} \text{yr}^{-1}$  in LAEs at  $z \approx 5$  (Pirzkal et al. 2007). A similar average value of SFR  $\approx 6 M_{\odot} \text{yr}^{-1}$  was inferred for  $z = 3.1$  LAEs (Gawiser et al. 2006). A slightly higher value of SFR  $\approx 5.7 - 28.3 M_{\odot} \text{yr}^{-1}$  with median SFR  $\approx 9.6 M_{\odot} \text{yr}^{-1}$  was inferred for  $z = 5.7$  LAEs (Murayama et al. 2007). For  $z = 6.6$  LAEs, Taniguchi et al. (2005) found an average SFR  $\approx 5.7 \pm 2.3 M_{\odot} \text{yr}^{-1}$ . These averages however

depend on the depth of the surveys; deeper surveys probe less luminous galaxies and hence lower SFRs. The total stellar mass in young stars (estimated using Equation (3)) of LAEs corresponding to the observed Ly $\alpha$  luminosity range is  $M_{\star} \approx (3 \times 10^7) - (3 \times 10^8) M_{\odot}$  in good agreement with the observed stellar masses  $\approx 10^7 M_{\odot} - 10^9 M_{\odot}$  of LAEs (Finkelstein et al. 2007; Gawiser et al. 2007; Pirzkal et al. 2007; Pentericci et al. 2009). Thus, our model reproduces the primary physical properties of LAEs at  $z \approx 3 - 7$ . In addition, our assumption of large escape fraction of Ly $\alpha$  photons will yield high observed EWs of Ly $\alpha$  line in LAEs (Malhotra & Rhoads 2002; Kudritzki et al. 2000; Dawson et al. 2004, 2007; Shimasaku et al. 2006; Wang et al. 2009).

### 5.2. Dust mass in our model LAEs

In our model we assume that LAEs do not contain significant amount of dust; however, we can estimate dust masses for our model LAEs using the dust estimates from SNe (Bianchi & Schneider 2007). Assuming a SNe rate  $\approx 1/150 M_{\odot}$  (Scannapieco & Bildsten 2005) and that each SN produces  $\sim 0.1 - 0.6 M_{\odot}$  of dust (Bianchi & Schneider 2007) of which nearly 2%–20% survives (Bianchi & Schneider 2007), we estimate a dust mass  $M_{\text{dust}} \approx (4 \times 10^3) - (2 \times 10^5) M_{\odot}$  for our model LAEs with SFR  $\approx 10 M_{\odot} \text{yr}^{-1}$ .

We now compare these values with the dust mass of LAEs inferred from observations. With extinction of  $A_V = 0.1 - 1.5$  for LAEs at  $z \approx 4.5$  (Finkelstein et al. 2008), with their sizes of 1 kpc in radii (Bond 2009, S. Malhotra et al 09 in preparation), and assuming a dust to gas ratio of 1/200, we estimate a dust mass

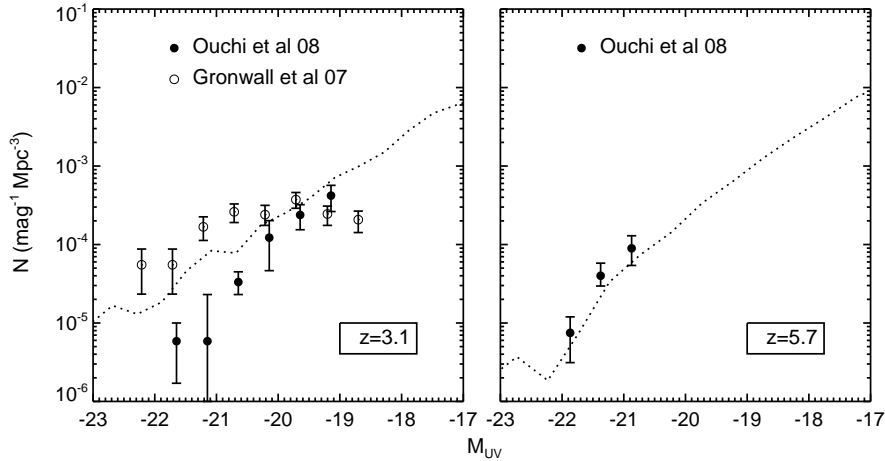


FIG. 4.— UV LFs of LAEs at  $z = 3.1$  and  $z = 5.7$ . The filled and open circles are the data from Ouchi et al. (2008) & Gronwall et al. (2007), respectively. The dotted line is our model predicted UV LF of LAEs.

$\approx (3 \times 10^4) - (4.5 \times 10^5) M_{\odot}$ , in agreement with the estimated values for our model LAEs. There are, however, considerable uncertainties in both, observational and theoretical estimates of dust mass.

### 5.3. UV Luminosity Function of LAEs

Our model, with single parameter, *i.e.*, the SFE, reproduced the observed Ly $\alpha$  LFs over a wide range of redshifts,  $z = 3 - 7$ . Now we compare the UV LFs of our model LAEs with the observations at  $z = 3.1$  (Gronwall et al. 2007; Ouchi et al. 2008) and  $z = 5.7$  (Ouchi et al. 2008). We convert Ly $\alpha$  luminosity to UV luminosity using the following relation (Madau et al. 1998)

$$L_{UV}(\text{ergs}^{-1} \text{Hz}^{-1}) = 8 \times 10^{27} \times \text{SFR}(M_{\odot} \text{yr}^{-1}), \quad (6)$$

where  $L_{UV}$  is the UV luminosity at  $1500\text{\AA}$ , and SFR is the star formation rate of our model LAEs calculated using Equation (2). Figure 4 shows the comparison between model predicted and observed UV LFs at  $z = 3.1$  and  $z = 5.7$ . Filled and open circles are the observations from Ouchi et al. (2008) and Gronwall et al. (2007), respectively, while the dotted line is our model predicted UV LF. At  $z = 5.7$ , the model predicted UV LF agrees quite well with the observations, while at  $z = 3.1$ , the observed UV LFs of Ouchi et al. (2008) and Gronwall et al. (2007) brackets our model predicted UV LF.

### 5.4. Evolution of Ly $\alpha$ luminosity function

The Ly $\alpha$  LFs have been used to probe the epoch of reionization and constrain the evolution of intergalactic medium (IGM) (e.g. Haiman & Spaans 1999; Malhotra & Rhoads 2004; Haiman & Cen 2005; Stern et al. 2005; Kashikawa et al. 2006; Dijkstra et al. 2007; McQuinn et al. 2007; Mesinger & Furlanetto 2008; Ota et al. 2008). Any significant evolution in the number density of LAEs, after accounting the newly formed LAEs between two redshifts will imply that the IGM evolved at these redshifts.

Currently, the evolution of Ly $\alpha$  LF at  $z > 5$  is not well understood. Previous studies find no significant evolution in Ly $\alpha$  LFs at redshifts between  $z = 5.7$  and

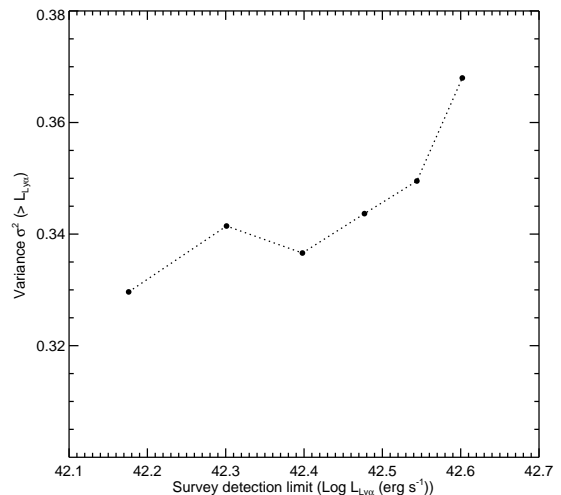


FIG. 5.— Field-to-field variance of number of LAEs at  $z = 6.6$ , measured in eight subvolumes ( $102 \times 51 \times 25 \text{ Mpc}^3$ ), plotted as a function of survey detection limit. The variance  $\sigma^2 > 30\%$  for a typical narrowband LAE survey with Ly $\alpha$  detection limit  $> 2 \times 10^{42} \text{ erg s}^{-1}$ .

$z = 6.5$  (Malhotra & Rhoads 2004). However recent observations (Kashikawa et al. 2006; Ota et al. 2008) find a modest decline in the bright end of the Ly $\alpha$  LF from  $z = 5.7$  to  $z = 6.6$  suggesting IGM evolution at these redshifts. Dijkstra et al. (2007) showed that the weak Ly $\alpha$  LF evolution between  $z = 5.7$  &  $z = 6.6$  can be attributed to the evolution of DM halo mass function. In addition, the cosmic variance in a volume limited LAE survey also affects the Ly $\alpha$  LF. For example, Shioya et al. (2009) find that the number density of LAEs, at  $z \approx 5$  vary by a factor  $\approx 2$  in a survey area of  $0^\circ.5 \times 0^\circ.5$ . We now investigate the evolution of Ly $\alpha$  LFs, and the effect of cosmic variance on number density of LAEs in a volume and flux limited LAE survey.

From Fig. 2 we see that there is some evolution of number density of DM halos that can host LAEs. However, this weak evolution is due to the intrinsic change in the number density since we have not included any IGM correction in our model. Thus our model can explain the observed evolution of Ly $\alpha$  LF (Kashikawa et al. 2006)

without invoking sample variance or reionization. We now estimate the effect of sample variance on the Ly $\alpha$  LF.

In order to understand the effect of cosmic variance on the observed number density of LAEs in a volume and flux limited LAE survey, we estimate the field-to-field variance by dividing the total simulation volume into eight non-overlapping rectangular boxes, each with a comoving volume ( $102 \times 51 \times 25$  Mpc $^3$ ) comparable to typical narrow-band LAE surveys ( $\approx 2 \times 10^5$  Mpc $^3$ ). The variance is calculated using  $\sigma^2 = \langle (N - \mu)^2 \rangle / \mu$ , where  $N$  is the number of LAEs in each sub-volume and  $\mu$  is the average number of LAEs. Figure 5 shows field-to-field variance, for a volume limited LAE survey with different Ly $\alpha$  flux limit. For a narrow-band LAE survey with Ly $\alpha$  detection limit of  $L_{\text{Ly}\alpha} > 2 \times 10^{42}$  erg s $^{-1}$  and a survey volume  $< 2 \times 10^5$  Mpc $^3$ , the field-to-field variation is significant with  $\sigma^2 \gtrsim 30\%$ . This result confirms the necessity of using a large volume to minimize sample variance in LAE surveys. It also strengthens our conclusion that some apparent evolution of Ly $\alpha$  LF can be attributed to the sample variance.

## 6. CLUSTERING OF LAES

Previous studies (e.g. Iliev et al. 2008; Orsi et al. 2008) suggest that LAEs trace rarer and higher density regions. However, Shimizu et al. (2007) suggested that the LAEs at  $z \approx 3$  do not necessarily reside in high density peaks. In this section, we investigate whether our model LAEs reside in high density regions and estimate their spatial correlation lengths. Figure 6 shows the spatial distribution of LAEs at two different redshifts,  $z = 5.7$  and  $z = 4.5$ , in a simulation slice of  $30 \times 30 \times 17$   $h^{-3}$  Mpc $^3$ . The depth of this slice is comparable to the depth of a typical LAE survey. Comparing the locations of LAEs at two redshifts it is clear that different halos host LAEs at different redshifts, thus exhibiting a duty cycle (Kovač et al. 2007; Stark et al. 2007; Nagamine et al. 2008). Our model LAEs are generally located around overdense regions consistent with the observations and as expected in biased galaxy formation models.

### 6.1. Two-point spatial correlation function

The two-point spatial correlation function  $\xi(r)$  (Peebles 1980) is frequently used to study the clustering properties of galaxies (e.g., Zehavi et al. 2005; Gawiser et al. 2007; Kovač et al. 2007). We use the Landy-Szalay estimator, proposed by Landy & Szalay (1993), to calculate the two-point spatial correlation function given by

$$\xi(r) = \frac{DD(r) - 2DR(r) + RR(r)}{RR(r)}, \quad (7)$$

where  $DD(r)$ ,  $RR(r)$ , and  $DR(r)$  are the number of galaxy-galaxy, random-random, and galaxy-random pairs, respectively with separation distance of  $(r, r + \delta r)$ . To compare our model  $\xi(r)$  with the observations and quantify its evolution with redshift we only include LAEs brighter than the detection limit of LAE surveys at a given redshift, and use our full simulation volume  $\approx 1 \times 10^6$  Mpc $^3$  for better statistical significance.

To calculate  $\xi(r)$  at each redshift, we generated a random sample of points with uniform coordinates drawn

from a uniform probability distribution, and a number of random points exactly equal to the number of LAEs. We count the number of pairs,  $DD(r)$ ,  $RR(r)$ , and  $DR(r)$  separated by a distance  $r$  by binning the points at different  $r$  with binwidth of  $\delta r = 0.2 h^{-1}$  Mpc. To minimize the random errors, we perform 50 realizations with different sets of random points and calculate an average  $\xi(r)$  at each  $r$ . Using  $r < 20$   $h^{-1}$  Mpc and assuming negligible error, we obtain the spatial correlation length  $r_0$  by fitting a least-square power law to the correlation function.

The correlation lengths obtained from our model LAEs show a modest evolution, with  $r_0 = (3.2 \pm 0.3, 5.0 \pm 0.3, 4.2 \pm 0.6, 6.0 \pm 1) h^{-1}$  at  $z = (3.1, 4.5, 5.7, 6.6)$ , respectively. Figure 7 (left) shows a comparison between our model predictions (filled circles) and observed  $r_0$  (shown with different symbols given in the labels) at different redshifts. The model predicted  $r_0$  values are slightly shifted along x-axis to avoid overlap with the observations. The predicted correlation lengths are consistent with the observations at  $z = 3.1$  with observed  $r_0 = 2.6 \pm 1$   $h^{-1}$  (Gawiser et al. 2007), and at  $z = 4.5$  with observed  $r_0 = 4.6 \pm 0.6$   $h^{-1}$  (Kovač et al. 2007) estimated using contamination-corrected (the maximum value permitted) LAE sample. However, Ouchi et al. (2003) found a higher  $r_0 = 6.2 \pm 0.5$   $h^{-1}$  Mpc for contamination-corrected LAE sample  $z = 4.86$ . We now estimate the variance of  $r_0$  in a volume and flux limited LAE survey, and see if we can account for the large difference seen in the observed  $r_0$  between  $z = 4.5$  &  $z = 4.86$  LAE surveys.

To estimate the variance of  $r_0$  ( $\sigma_{r_0}^2$ ) in a volume and flux limited LAE survey, we divide the total simulation volume at  $z = 3.1$  into five non-overlapping sub-volumes, each with a comoving volume of  $(102 \times 102 \times 20.4)$  Mpc $^3$ , approximately equal to a typical survey volume and only including LAEs with  $L_{\text{Ly}\alpha} > 1 \times 10^{42}$  erg s $^{-1}$ . We calculate  $\xi(r)$  and  $r_0$ , as described above (second paragraph) in each sub-volume and estimate  $\sigma_{r_0}^2$  at  $z = 3.1$ . We find  $\sigma_{r_0}^2 = 0.5$   $h^{-1}$  Mpc with an average  $r_0 = 3.2$   $h^{-1}$  Mpc, average of  $r_0$  in five sub-volumes. While this variance in  $r_0$  cannot account for the large difference in  $r_0$  observed between the two surveys at  $z = 4.5$  &  $4.86$ , it is clear that one needs to take into account such variance in correlation lengths obtained from volume and flux limited surveys.

Finally we investigate if the redshift evolution of  $r_0$  seen in Figure 7 (left panel) is significant since this can result from the surveys at lower redshifts extending to lower luminosities and hence probing lower halo masses. In order to understand this effect, we consider full simulation volume and only include LAEs with a constant  $L_{\text{Ly}\alpha} > 1 \times 10^{42}$  erg s $^{-1}$  at all redshifts. Choosing a constant luminosity cutoff at all redshifts implies that we are probing approximately same halo masses at all redshifts. We calculate  $r_0$  in the same way as described above (second paragraph) except that we impose the same luminosity cutoff at all redshifts. Figure 7 (right panel) shows  $r_0$  with a constant lower luminosity at all redshifts. Most of this evolution seen in Figure 7 (left panel) can be attributed to the luminosity limit of different surveys probing different halo masses.

## 7. SUMMARY AND CONCLUSIONS

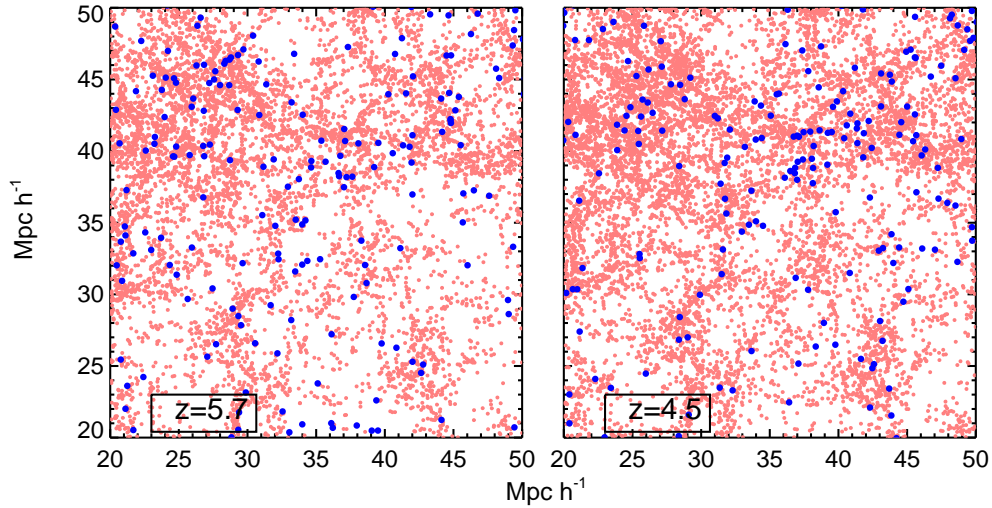


FIG. 6.— The spatial distribution of our model LAEs in a slice from DM simulation at two redshifts  $z = 5.7$  (left) and  $z = 4.5$  (right) in a volume  $30 \times 30 \times 17 \ h^{-3} \text{ Mpc}^3$ . The small (red) and big (blue) filled circles represent the positions of DM halos and model LAEs, respectively. Only LAEs with  $L_{\text{Ly}\alpha} > 2 \times 10^{42} \text{ erg s}^{-1}$  are plotted. In general, the LAEs are located in high density regions. Also note that different halos host LAEs at the two redshifts, depending on whether they are accreting or not. This gives rise to a duty cycle quite naturally.

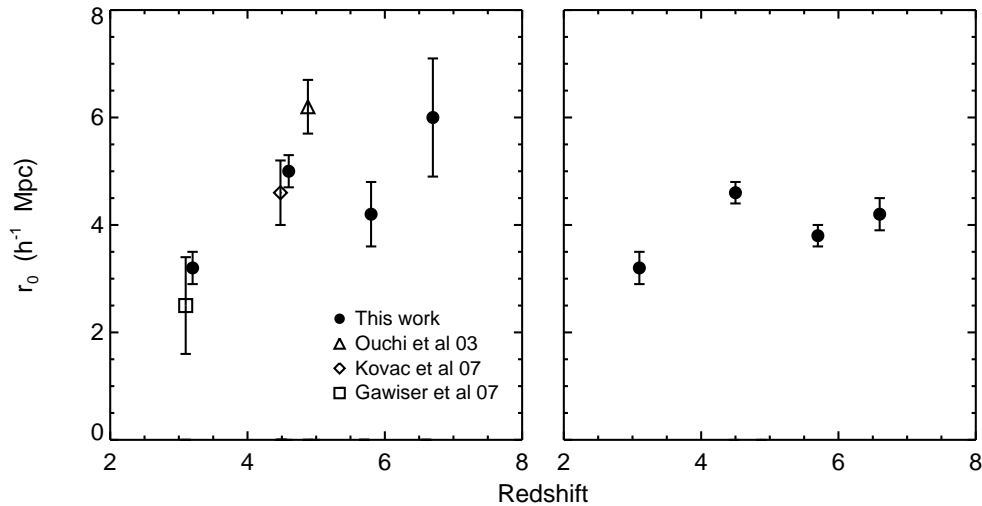


FIG. 7.— Correlation lengths of LAEs at different redshifts. *Left*. Comparison of correlation lengths of our model and observed LAEs at different redshifts. Here we include LAEs with  $\text{Ly}\alpha$  luminosity greater than the survey limit at each redshift. The filled circles are our model results, other symbols are from different observations as shown in the labels. The observed  $r_0$  values shown here for  $z=4.5$  &  $4.86$  are for the contamination corrected (the maximum value permitted) LAE sample. Our model results are slightly shifted to avoid overlap with other observational points. *Right*: The correlation lengths of our model LAEs with a constant  $\text{Ly}\alpha$  luminosity cutoff ( $L_{\text{Ly}\alpha} > 1 \times 10^{42} \text{ erg s}^{-1}$ ) at all redshifts, showing that the apparent evolution of correlation length with redshift (seen in left panel) is mostly due to different luminosity detection limits in LAE surveys.

We have used a physical model with a single variable parameter to populate DM halos with LAEs in a cosmological simulation and compared our model predictions with the observations at redshifts  $z \approx 3 - 7$ . In our model, we assumed that the SFR, and hence the  $\text{Ly}\alpha$  line luminosity is proportional to the mass accreted by halos. In other words, the star formation in LAEs mainly results from the accretion of new material. Despite the

lack of observational evidence relating accretion rate to the  $\text{Ly}\alpha$  luminosity of LAEs, it is promising that our model gives a good fit to the observations over a wide range of redshifts and is able to reproduce several other physical properties of LAEs. In addition, relating the accreted mass rather than the total halo mass to the  $\text{Ly}\alpha$  luminosity gives rise to a duty cycle of LAEs quite naturally.



To compare our model predictions with observations, we first constructed the Ly $\alpha$  LF at  $z = 3.1$  and obtained the best-fit model by varying the SFE and comparing the model Ly $\alpha$  LF with the observations at this redshift. We then used this best-fit model to predict the Ly $\alpha$  LFs and physical properties of LAEs at  $z = 4.5, 5.7$  and  $z = 6.6$ .

Using a constant SFE, our model predicted Ly $\alpha$  LFs agree remarkably well with the LAE observations over a wide redshift range. Our best-fit model yields a SFE = 2.5% which gives SFR  $\approx 1 - 10 M_{\odot}\text{yr}^{-1}$  in good agreement with the observations. We find that the model LAEs in the currently observable luminosity range ( $2 \times 10^{42} \lesssim L_{\text{Ly}\alpha} \lesssim 2 \times 10^{43} \text{erg s}^{-1}$ ) have stellar masses  $\approx 3 \times 10^7$  to  $3 \times 10^8 M_{\odot}$  of young ( $< 30$  Myr) stars. These stellar masses of LAEs are similar to those inferred from observations (Finkelstein et al. 2007; Pirzkal et al. 2007). We have estimated the dust mass  $M_{\text{dust}} \approx (4 \times 10^3) - (2 \times 10^5) M_{\odot}$  for our model LAEs with  $L_{\text{Ly}\alpha} = 1 \times 10^{43} \text{erg s}^{-1}$ , in agreement with the inferred dust masses  $\approx (3 \times 10^4) - (4.5 \times 10^5) M_{\odot}$  from LAE observations at  $z \approx 4.5$  (Finkelstein et al. 2008). Using our model LAEs, we constructed UV LF and compared it with the observations at  $z = 3.1$  and  $z = 5.7$ . At  $z = 5.7$ , our model predicted UV LF of LAEs agrees quite well with the observations, while at  $z = 3.1$ , the observed UV LFs of Gronwall et al. (2007) and Ouchi et al. (2008) bracket our model-predicted UV LF.

While our model predicts a constant SFE, and hence a weak evolution of other physical properties of LAEs over a redshift range  $z = 3-7$ , this value also depends on the ratio of baryons to DM. Thus, in reality  $f_{\star}$ , and hence other physical properties of LAEs might show detectable, albeit weak, evolution with redshift.

We also investigated the evolution of Ly $\alpha$  LFs from  $z \approx 3 - 7$  and find that there is no significant evolution of Ly $\alpha$  LF due to the IGM if we include the intrinsic

change in the number density of LAEs over this redshift range. This conclusion is strengthened if we include the effect of cosmic variance on the observed number density of LAEs. We show that the field-to-field variance can be large  $\approx 30\%$  for a flux and volume limited surveys comparable to current observations.

We studied the clustering properties of LAEs and found that the LAEs are mostly located in the high density peaks. Our model predicted correlation lengths  $r_0 = (3.2 \pm 0.3, 5.0 \pm 0.3) h^{-1} \text{Mpc}$  which are in good agreement with the observations. We also estimate the variance ( $\sigma_{r_0}^2$ ) in  $r_0$  for a volume and flux limited LAE survey and find that  $\sigma_{r_0}^2 = 0.5 h^{-1} \text{Mpc}$  at  $z = 3.1$ . Our models predict a modest evolution of the correlation length with redshift. Currently, there are no measurements of  $r_0$  at  $z > 5$  due to insufficient sample size of LAEs at higher redshifts. Therefore, more data are needed to test our predictions at higher redshifts in order to understand the evolution of  $r_0$  with redshifts.

We acknowledge helpful suggestions from Kyoung-Soo Lee. We are also grateful to the anonymous referee for insightful comments and suggestions. This work was supported in part by the School of Earth & Space Exploration, Arizona State University, the NSF grant AST-0808165, the Swiss National Science Foundation grant 200021-116696/1, and Swedish Research Council grant 60336701. R. J. T. is supported by a Discovery Grant from NSERC, the Canada Research Chairs program and the Canada Foundation for Innovation. All simulations were conducted on the *Saguaro* cluster operated by the Fulton School of Engineering at Arizona State University. This research has made use of NASA's Astrophysics Data System.

## REFERENCES

- Ajiki, M., et al. 2003, *AJ*, 126, 2091  
 Baldry, I. K., Glazebrook, K., & Driver, S. P. 2008, *MNRAS*, 388, 945  
 Barton, E. J., Davé, R., Smith, J.-D. T., Papovich, C., Hernquist, L., & Springel, V. 2004, *ApJ*, 604, L1  
 Bianchi, S., & Schneider, R. 2007, *MNRAS*, 378, 973  
 Bond, N. 2009, *New Astronomy Review*, 53, 42  
 Cowie, L. L., & Hu, E. M. 1998, *AJ*, 115, 1319  
 Crocce, M., Pueblas, S., & Scoccimarro, R. 2006, *MNRAS*, 373, 369  
 Davé, R., Finlator, K., & Oppenheimer, B. D. 2006, *MNRAS*, 370, 273  
 Davis, M., Efstathiou, G., Frenk, C. S., & White, S. D. M. 1985, *ApJ*, 292, 371  
 Dawson, S., et al. 2004, *ApJ*, 617, 707  
 Dawson, S., Rhoads, J. E., Malhotra, S., Stern, D., Wang, J., Dey, A., Spinrad, H., & Jannuzi, B. T. 2007, *ApJ*, 671, 1227  
 Dayal, P., Ferrara, A., & Gallerani, S. 2008, *MNRAS*, 389, 1683  
 Dekel, A., Sari, R., & Ceverino, D. 2009, *arXiv:0901.2458*  
 Dijkstra, M., Haiman, Z., & Spaans, M. 2006, *ApJ*, 649, 14  
 Dijkstra, M., Wyithe, J. S. B., Haiman, Z. 2007, *MNRAS*, 379, 253D  
 Fardal, M. A., Katz, N., Gardner, J. P., Hernquist, L., Weinberg, D. H., & Davé, R. 2001, *ApJ*, 562, 605  
 Fernandez, E. R., & Komatsu, E. 2008, *MNRAS*, 384, 1363  
 Finkelstein, S. L., Rhoads, J. E., Malhotra, S., Pirzkal, N., & Wang, J. 2007, *ApJ*, 660, 1023  
 Finkelstein, S. L., Rhoads, J. E., Malhotra, S., Grogan, N., & Wang, J. 2008, *ApJ*, 678, 655  
 Fukugita, M., Hogan, C. J., & Peebles, P. J. E. 1998, *ApJ*, 503, 518  
 Fynbo, J. U., Möller, P., & Thomsen, B. 2001, *A&A*, 374, 443  
 Gawiser, E., et al. 2006, *ApJ*, 642, L13  
 Gawiser, E., et al. 2007, *ApJ*, 671, 278  
 Gawiser, E., et al. 2007, *ApJ*, 671, 278  
 Genel, S., et al. 2008, *ApJ*, 688, 789  
 Gnedin, N. Y., Kravtsov, A. V., & Chen, H.-W. 2008, *ApJ*, 672, 765  
 Gronwall, C., et al. 2007, *ApJ*, 667, 79  
 Haiman, Z., & Spaans, M. 1999, *ApJ*, 518, 138  
 Haiman, Z., Spaans, M., & Quataert, E. 2000, *ApJ*, 537, L5  
 Haiman, Z., & Cen, R. 2005, *ApJ*, 623, 627  
 Hansen, M., & Oh, S. P. 2006, *MNRAS*, 367, 979  
 Hinshaw, G., et al. 2009, *ApJS*, 180, 225  
 Hu, E. M., McMahon, R. G., & Cowie, L. L. 1999, *ApJ*, 522, L9  
 Iliev, I. T., Shapiro, P. R., McDonald, P., Mellema, G., & Pen, U.-L. 2008, *MNRAS*, 391, 63  
 Jimenez, R., Panter, B., Heavens, A. F., & Verde, L. 2005, *MNRAS*, 356, 495  
 Kashikawa, N., et al. 2006, *ApJ*, 648, 7  
 Kereš, D., Katz, N., Fardal, M., Davé, R., & Weinberg, D. H. 2009, *MNRAS*, 395, 160  
 Kobayashi, M. A. R., Totani, T., & Nagashima, M. 2007, *ApJ*, 670, 919  
 Kobayashi, M. A. R., Totani, T., & Nagashima, M. 2009, *arXiv:0902.2882*  
 Kovač, K., Somerville, R. S., Rhoads, J. E., Malhotra, S., & Wang, J. 2007, *ApJ*, 668, 15  
 Kudritzki, R.-P., et al. 2000, *ApJ*, 536, 19

- Landy, S. D., & Szalay, A. S. 1993, *ApJ*, 412, 64
- Le Delliou, M., Lacey, C. G., Baugh, C. M., & Morris, S. L. 2006, *MNRAS*, 365, 712
- Leitherer, C., Ferguson, H. C., Heckman, T. M., & Lowenthal, J. D. 1995, *ApJ*, 454, L19
- Madau, P., Pozzetti, L., & Dickinson, M. 1998, *ApJ*, 498, 106
- Malhotra, S., & Rhoads, J. E. 2002, *ApJ*, 565, L71
- Malhotra, S., Wang, J. X., Rhoads, J. E., Heckman, T. M., & Norman, C. A. 2003, *ApJ*, 585, L25
- Malhotra, S., & Rhoads, J. E. 2004, *ApJ*, 617, L5
- Mao, J., Lapi, A., Granato, G. L., de Zotti, G., & Danese, L. 2007, *ApJ*, 667, 655
- Matsuda, Y., et al. 2005, *ApJ*, 634, L125
- McQuinn, M., Hernquist, L., Zaldarriaga, M., & Dutta, S. 2007, *MNRAS*, 381, 75
- Mesinger, A., & Furlanetto, S. R. 2008, *MNRAS*, 386, 1990
- Murayama, T., et al. 2007, *ApJS*, 172, 523
- Nagamine, K., Ouchi, M., Springel, V., & Hernquist, L. 2008, *arXiv:0802.0228*
- Nagao, T., et al. 2008, *ApJ*, 680, 100
- Nilsson, K. K., et al. 2007, *A&A*, 471, 71
- Orsi, A., Lacey, C. G., Baugh, C. M., & Infante, L. 2008, *MNRAS*, 391, 1589
- Ota, K., et al. 2008, *ApJ*, 677, 12
- Ouchi, M., et al. 2008, *ApJS*, 176, 301
- Ouchi, M., et al. 2003, *ApJ*, 582, 60
- Partridge, R. B., & Peebles, P. J. E. 1967, *ApJ*, 147, 868
- Peebles, P. J. E. 1980, Research supported by the National Science Foundation. Princeton, N.J., Princeton University Press, 1980. 435 p
- Pentericci, L., Grazian, A., Fontana, A., Castellano, M., Giallongo, E., Salimbeni, S., & Santini, P. 2009, *A&A*, 494, 553
- Pirzkal, N., Malhotra, S., Rhoads, J. E., & Xu, C. 2007, *ApJ*, 667, 49
- Razoumov, A. O., & Sommer-Larsen, J. 2006, *ApJ*, 651, L89
- Rhoads, J. E., Malhotra, S., Dey, A., Stern, D., Spinrad, H., & Jannuzi, B. T. 2000, *ApJ*, 545, L85
- Rhoads, J. E., & Malhotra, S. 2001, *ApJ*, 563, L5
- Rhoads, J. E., et al. 2004, *ApJ*, 611, 59
- Samui, S., Srianand, R., & Subramanian, K. 2009, *arXiv:0906.2312*
- Scannapieco, E., & Thacker, R. J. 2003, *ApJ*, 590, L69
- Scannapieco, E., & Bildsten, L. 2005, *ApJ*, 629, L85
- Shapley, A. E., Steidel, C. C., Pettini, M., Adelberger, K. L., & Erb, D. K. 2006, *ApJ*, 651, 688
- Shimizu, I., Umemura, M., & Yonehara, A. 2007, *MNRAS*, 380, L49
- Shioya, Y., et al. 2009, *ApJ*, 696, 546
- Shimasaku, K., et al. 2006, *PASJ*, 58, 313
- Spergel, D. N., et al. 2007, *ApJS*, 170, 377
- Springel, V. 2005, *MNRAS*, 364, 1105
- Stark, D. P., Loeb, A., & Ellis, R. S. 2007, *ApJ*, 668, 627
- Stern, D., Yost, S. A., Eckart, M. E., Harrison, F. A., Helfand, D. J., Djorgovski, S. G., Malhotra, S., & Rhoads, J. E. 2005, *ApJ*, 619, 12
- Tapken, C., et al. 2006, *A&A*, 455, 145
- Taniguchi, Y., et al. 2005, *PASJ*, 57, 165
- Tasitsiomi, A. 2006, *ApJ*, 645, 792
- Thacker, R. J. & Couchman, H. M. P., 2006, *Int. J. High Perf. Comp. & Net.*, 4, 303
- Venemans, B. P., et al. 2005, *A&A*, 431, 793
- Wang, J. X., et al. 2004, *ApJ*, 608, L21
- Wang, J. X., Malhotra, S., & Rhoads, J. E. 2005, *ApJ*, 622, L77
- Wang, J.-X., Malhotra, S., Rhoads, J. E., Zhang, H.-T., & Finkelstein, S. L. 2009, *arXiv:0907.0015*
- Wood, K., & Loeb, A. 2000, *ApJ*, 545, 86
- Zehavi, I., et al. 2005, *ApJ*, 630, 1